Available online at www.sciencedirect.com
SCIENCE DIRECT®
Computers, Environment and Urban Systems
29 (2005) 501–523
Computers, Environment and Urban Systems
www.elsevier.com/locate/compenvurbsys

A study of lacunarity-based texture analysis approaches to improve urban image classification

Soe Win Myint [a,*], Nina Lam [b]

[a] Department of Geography, 100 East Boyd Street, University of Oklahoma, Norman, OK 73019, USA
[b] Department of Geography and Anthropology, 227 Howe/Russell Geoscience Complex, Louisiana State University, Baton Rouge, LA 70803, USA

Abstract

The traditional spectral based classifiers are normally considered ineffective in digitally classifying urban land-use and land-cover classes from high-resolution remotely sensed data due to the lack of consideration of images' spatial properties. To identify the complex arrangements of urban features in high-resolution image data, the texture information contained in a group of pixels needs to be considered. This paper discusses the concept of lacunarity and the use of two lacunarity estimation methods (i.e., binary, gray scale) in texture analysis and classification of urban images. Lacunarity has been introduced to characterize different texture appearances, which may share the same fractal dimension value. Lacunarity measures the distribution of gap sizes: low lacunarity geometric objects are homogeneous because all gap sizes are the same, whereas high lacunarity objects are heterogeneous. Using different moving windows (i.e., 13×13, 21×21, 29×29), the above lacunarity methods were employed to classify urban features and to observe the effects of the size of moving windows in characterizing urban texture features. Results from this study show that traditional spectral based classification approach is inaccurate in classifying urban land categories from high-resolution image data, with an accuracy of 55%, whereas lacunarity approaches can be used to improve urban classification accuracy dramatically to 92%.

* Corresponding author.
E-mail addresses: swmyint@ou.edu (S.W. Myint), nlam@lsu.edu (N. Lam).

0198-9715/$ - see front matter
doi:10.1016/j.compenvurbsys.2005.01.007

Keywords: Lacunarity; Texture; Urban

1. Introduction

The conventional per-pixel image classification techniques have proven ineffective due to the lack of consideration of images' spatial information in digitally classifying the urban land-use and land-cover features in high-resolution images (Green, Cummins, Wright, & Miles, 1993; Kiema & Bahr, 2001; Muller, 1997; Myint, Lam, & Tyler, in press). It is obvious that the higher the spatial resolution of remotely sensed data we employ, the higher the level of detailed objects and features in urban areas (e.g., houses, trees, shrubs, driveways, grass, sidewalks, bare-soil, tar roads, cement roads, etc.) can be detected. Hence, the spectral response from different land-cover features from an urban environment as a whole in high-resolution images always exhibit spatial complexity (Myint et al., in press).

Moreover, urban features are composed of spectrally different various materials (e.g., plastic, metal, rubber, glass, cement, wood, etc.) concentrated in a small area (Jensen & Cowen, 1999). The high frequency spatial appearance of urban land-cover features is a major limitation in accurately classifying urban land-use and land-cover classes in high-resolution image data (Myint, Lam, & Tyler, 2002). The classification accuracy of images is the result of a trade-off between two main factors: class boundary pixels and within-class variances (Metzger & Muller, 1996). Most common image processing algorithms do not take the local structure or the spatial arrangement of neighborhood pixels into consideration. To extract the heterogeneous nature of urban features in high-resolution images, the texture information contained in a group of neighborhood pixels needs to be considered. Traditional spectral classification algorithms use individual pixel values and ignore spatial information. This spatial information is crucial in urban mapping when using high-resolution images, because most of the urban classes contain a number of spectrally different features or objects arranged in complex spatial forms (e.g., trees, grass, shrubs, driveways, sidewalks, parking lots, cement roads, tar roads, houses, office buildings).

Another limiting factor for accurate urban classification is that it is extremely difficult to define suitable training sets for many categories within urban environments. This is due to variation in the spectral response of their component land-cover types (Barnsley, Barr, & Sadler, 1991). Therefore, the training statistics may exhibit very high standard deviation (Sadler, Barnsley, & Barr, 1991) and violate one of the basic assumptions of the widely used maximum-likelihood decision rule, namely, that the pixel values follow a multi-variate normal distribution (Barnsley et al., 1991; Sadler et al., 1991).

Various attempts, including some new spatial techniques, were made to improve the spectral analysis of remotely sensed data. Local variability in remotely sensed data can be characterized by computing the statistics of a group of pixels, e.g., coefficient of variance or autocovariance, or by the analysis of fractal relationships. There have been some attempts to improve the spectral analysis of remotely sensed data by using texture transforms in which some measure of variability in digital number (DN) values is estimated within local windows; e.g., contrast between neighboring pixels, the standard deviation, or local variance. The coefficient of variance also gives a measure of the total relative variation of pixel values in an area and can be computed easily, but it gives no information about spatial patterns. One commonly used statistical procedure for interpreting texture uses image spatial co-occurrence matrix, which is also known as gray level co-occurrence matrix (GLCM) (Haralick, Shanmugan, & Dinstein, 1973; Franklin, Hall, Moskal, Maudie, & Lavigne, 2000; Pesaresi, 2000). There are a number of texture measures, which could be applied to spatial co-occurrence matrices for texture analysis (Peddle & Franklin, 1991). Variograms of remotely sensed measurements can also be used to quantitatively describe the spatial patterns. Emerson, Lam, and Quattrochi (1999) analyzed the fractal dimension of satellite imagery using the Isarithm method and the spatial auto-correlation using Moran's I and Geary's C to observe the differing spatial structures of the smooth and rough features in remote sensing images. Myint et al. (2002, in press) used the technique of wavelet transform, a multi-scale textural method, to detect urban features, and they were able to obtain much higher level of classification accuracy. These various attempts of employing spatial techniques in urban land cover classification have shown promising results, which demonstrates convincingly the need for considering spatial information in urban land cover classification.

2. Lacunarity overview

The concept of lacunarity was originally developed by Mandelbrot (1983) to describe a property of fractals, and has since been extended to describe real data sets that may or may not have fractal and multi-fractal distributions (Plotnick, Gardner, Hargrove, Prestegaard, & Perlmutter, 1996). As such, understanding the development of fractals will aid in understanding lacunarity.

Fractal dimensions may be viewed as a measure of complexity or heterogeneity of spatial arrangements and physical processes in many fields of studies. There has been growing interest in the application of fractal geometry to characterize spatial complexity of geographic phenomena at multiple scales. The study of the relationship between physical processes and the effects of scale have become increasingly important in geographic information science. Mandelbrot (1983) defined the term fractal as "*a set for which the Hausdorff Besicovitch dimension strictly exceeds the topological dimension*." Fractals exemplify the idea of self-similarity, in which the spatial behavior of a system, an object or a group of features is independent of scale (Burrough, 1993; Turcotte, 1997). An ideal fractal curve or surface has a constant dimension value over all scales. The variability of many natural phenomena is often irregular and sometimes can be approximated by fractional Brownian motion (Mandelbrot, 1983). Details on the description of the fractal dimension measurement techniques can be observed in Jaggi, Quattrochi, and Lam (1993).

Some researchers anticipated that local fractal analysis of remotely sensed images may reveal information on different land-use and land-cover categories better than spectral based per-pixel classifier. A potential use of fractal dimension could be the analysis of texture information in image classification. Studies of image analysis and texture classification have been conducted by scholars in different disciplines over the past several decades with the expectation that different land-use and land-cover classes could be characterized by fractal dimension values (De Cola, 1989; De Jong & Burrough, 1995; Kaplan, 1999; Lam, 1990; Lam, Quattrochi, Qui, & Zhao, 1998; Lovejoy & Schertzer, 1990). While these analyses demonstrate the potential of fractal geometry in characterizing texture features in remotely sensed images, it was also pointed out that fractal analyses of constructed sets do not provide a complete description of natural scaling phenomena and remotely sensed images of the land-cover units are not true fractals (e.g., Burrough, 1989; De Jong & Burrough, 1995; Dong, 2000; Klinkenberg & Goodchild, 1992; Mark & Aronson, 1984; Myint, 2003a; Myint et al., 2002; Roach & Fung, 1994; Xia, 1993).

In fact, Mandelbrot (1995) reports that fractal dimensions are very far from providing a complete characterization of a set's texture. In other words, different fractal sets may share the same fractal dimension values but have different appearances or textures (Dong, 2000; Mandelbrot, 1983; Voss, 1986), just as different texture appearances of classes may share the same variance or mean value. As an initial step toward quantifying texture or spatial arrangements of features, Mandelbrot (1983) introduced the term lacunarity (lacunar is Latin for gap) to characterize different texture appearances, which may have the same fractal dimension value. Different fractal sets that have the same dimension value may be constructed, but they may look completely different because they have different lacunarity.

Lacunarity represents the distribution of gap sizes: low lacunarity geometric objects are homogeneous because all gap sizes are the same, whereas high lacunarity objects are heterogeneous (Dong, 2000). In other words, Lacunarity measures the deviation of a geometric structure from translational invariance, or gappiness of geometric structure (Gefen, Meir, & Aharony, 1983). It is important to note that objects that are homogeneous at a small scale can be heterogeneous at a larger scale (scale here refers to both measurement or window size and areal extent). Therefore, lacunarity is a scale-dependent measure of spatial complexity or texture of a landscape (Plotnick, Gardner, & O'Neill, 1993). Unlike most other landscapes indices and measures (Gustafson, 1998; Haines-Young & Chopping, 1996), the computed values of lacunarity are not sensitive to map boundaries but are sensitive to scale.

Because remote sensing images of urban landscape are full of textures and hardly self-similar, traditional spectral classification techniques, as well as fractals and other spatial indices applied at a single scale level, may not be able to capture the gaps and complexity of the landscape. Lacunarity is therefore applied in this study to examine if it increases the accuracy in classifying urban land cover features from high-resolution remote sensing images.

3. Data and study area

IKONOS image data at 4 m spatial resolution with four bands: blue (0.45–0.52 μm), green (0.52–0.60 μm), red (0.63–0.69 μm), and near infrared (0.76–

0.90 μm) acquired over Norman, OK on March 20, 2000 was used for classifying urban land use and land cover categories in this study. A subset of IKONOS data (1102×793 pixels) which contains the central part of the Norman metropolitan area is shown in Fig. 1 with a locator map. We used the original 11 bit data instead of converting it to 8 bit because it was anticipated that higher radiometric resolution

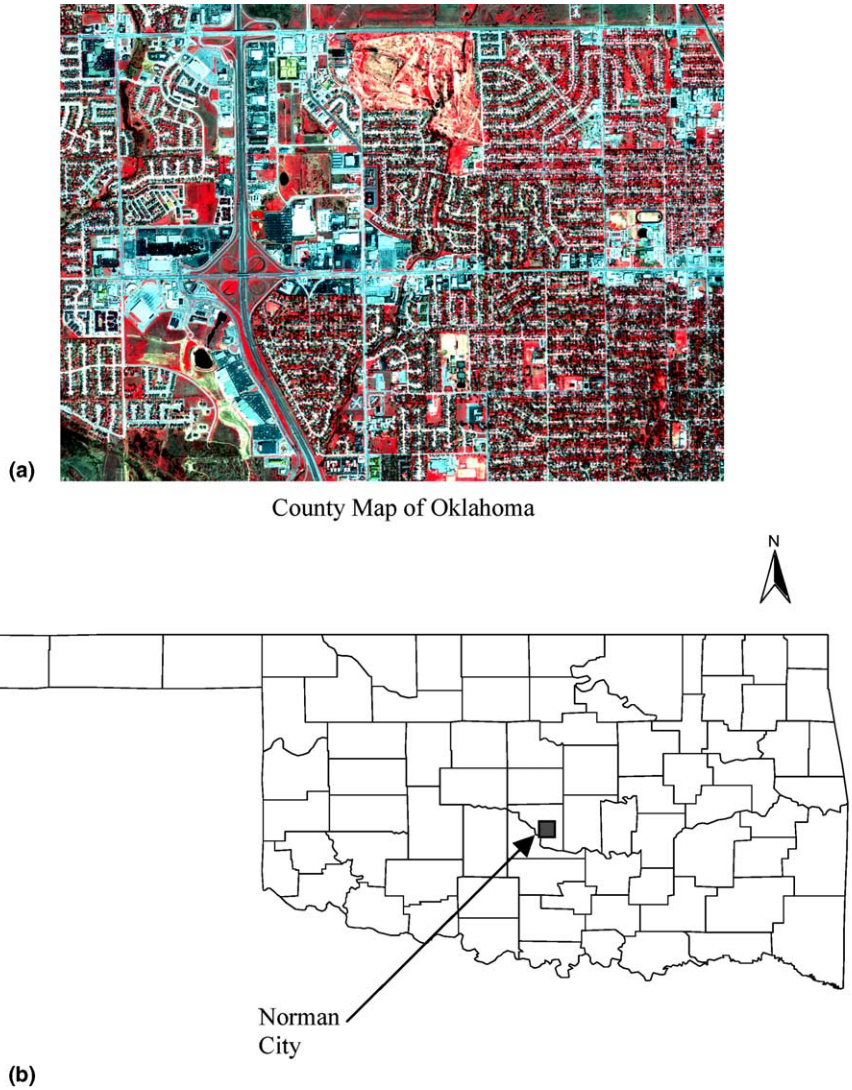

Fig. 1. (a) A subset of Norman, OK metropolitan area, displayed using bands 4 (0.76–0.90 μm) in red, bands 3 (0.63–0.69 μm) in green, and bands 2 (0.52–0.60 μm) in blue; (b) location of the study area (Norman city). (For interpretation of color in this figure legend the reader is referred to the web version of this article.)

would help us better identify texture features using lacunarity approaches. Examining the relationships between urban land-use land-cover classes associated with surface vegetation, water availability, and associated temperature fluctuation within an urban area is crucial for city planners and environmental officers. This information will be useful to developing a better infrastructure management plan to avoid environmental degradation: air pollution, noise pollution, traffic congestion, urban heat island effect, chemical contamination, and soil loss due to improper urban development and deforestation.

We considered residential areas with different tree crown closure percents as very important categories for urban planning. Vegetation influences urban environmental conditions and energy fluxes by selective reflection and absorption of solar radiation (Gallo et al., 1993) and by function of evapotranspiration (Owen, Carlson, & Gillies, 1998). The presence and abundance of vegetation in urban areas has long been recognized as a strong influence on energy demand and development of the urban heat island (Huang, Akbari, Taha, & Rosenfeld, 1987; Oke, 1982). Urban vegetation abundance may also influence air quality and human health (Wagrowski & Hites, 1997) because trees make their own food from carbon dioxide in the atmosphere, sunlight, water, and a little amount of soil elements, and release oxygen in the process. They also provide surface area for sequestration of particulate matter and ozone. The loss of trees in our urban areas intensifies the urban heat island effect due to the loss of shade and evaporation. In addition, we also lose the principal absorbers of carbon dioxide and trappers of other pollutants as well.

Hence, we attempted to identify two residential classes: one with less than 50% vegetation and the other one with vegetation more than 50%. The other classes included in this study were the only possible classes visually observed in the image over the study area. Following Lo, Quatrochi, and Luvall (1997), six urban land-use and land-cover features with different textural appearances were selected: single-family houses with less than 50% tree canopy (residential-1—R1), single-family houses with more than 50% tree canopy (residential-2—R2), commercial (C), woodland (F), agriculture (A), grassland (G), and water body (W). Bands 4 (near infrared), 3 (red), and 2 (green) were used as the original multi-spectral bands in this study.

4. Lacunarity approaches

Methods for calculating lacunarity were first introduced in general form by Mandelbrot (1983) and several other algorithms of computing lacunarity have been developed (Allain & Cloitre, 1991; Dong, 2000; Gefen et al., 1983; Lin & Yang, 1986; Voss, 1986). Allain and Cloitre (1991) initiated a conceptually straightforward and computationally simple "gliding box" algorithm for calculating lacunarity and reported that lacunarity appears to be a new tool for identifying the geometry of deterministic and random sets. Since lacunarity measures the heterogeneity or degree of contagion, a higher index value of lacunarity indicates a more heterogeneous feature or a more complex spatial arrangement, and vice versa. Plotnick et al. (1996) emphasized the concept and utilization of lacunarity for the characterization of spatial features, which may not be fractals. The gliding box algorithm has been used for calculating lacunarity value of binary images as well as gray-scale images. This paper evaluates both the binary and the gray-scale methods for computing lacunarity and their accuracy in classifying urban features. The two algorithms are described as follows.

4.1. Binary approach (gliding box method)

The gliding box of a specific size (r, length of a square box) is first placed at the top left corner of an image in which each and every pixel is filled with either 1 or 0 (Allain & Cloitre, 1991; Plotnick et al., 1993). We generate binary images by converting each gray-scale image (each band) into four quartile images with value 1's and 0's. We basically sliced the image into five levels in order to get the four quartile images. The location of each level can be computed using the following formula:

$$Q_l = (n)/(5/l) \tag{1}$$

where l $(1,\ldots,4)$ = location level, n = number of observations.

The digital value at the computed location for the first, second, third, and fourth levels were used as a threshold value to convert the original bands to binary images. For example, the binary image for the first quartile will turn pixels which have values above 75% of all pixels as 0's and the rest as 1's, and so on. If the first quartile breakpoint has a DN value of 41, all digital values above 41 (25% of all pixels) will be converted to zero and the rest will be assigned one. The transformed binary images of band 3 (i.e., Q_1, Q_2, Q_3, Q_4) are shown in Fig. 2(a)–(d). Texture transformed images of band 4, band 3, and band 2 derived from the lacunarity binary approach is hereafter called B_4, B_3, and B_2.

Then the box mass "S", the number of occupied pixels (1's), is computed. The gliding box is systematically moved through the binary image one pixel at a time and the box mass value is determined for each of the overlapping boxes. For lacunarity estimation of binary images, the gliding-box algorithm proposed by Allain and Cloitre (1991) and extended by Plotnick et al. (1993) is used. For a given box size r, the probability of box mass S is

$$P(S,r) = \frac{n(S,r)}{N(r)} \tag{2}$$

where $n(S,r)$ is the number of gliding box size r with mass S, and $N(r)$ is the total number of boxes of size r. The first and second moment of this distribution, $E(S)$ and $E(S^2)$ are

$$E(S) = \sum SP(S,r) \tag{3}$$

and

$$E(S^2) = \sum S^2P(S,r) \tag{4}$$

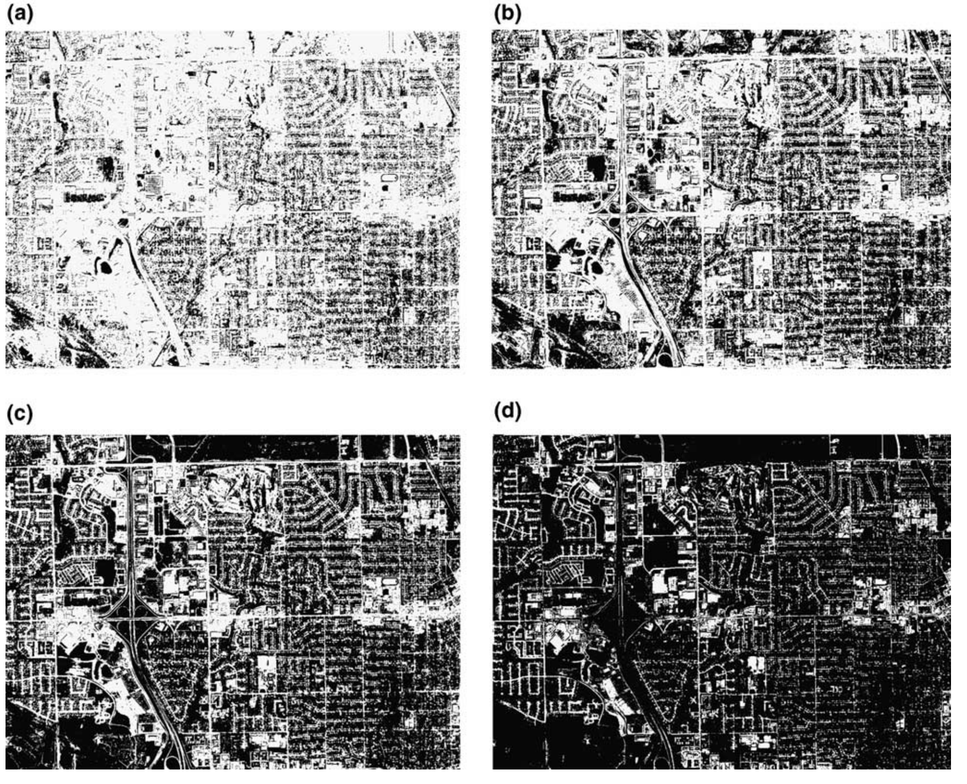

Fig. 2. Transformed binary images of band 3: Q_1 (a), Q_2 (b), Q_3 (c), and Q_4 (d).

Lacunarity for gliding box size r, $\Lambda(r)$, is defined as

$$\Lambda(r) = \frac{E(S^2)}{E^2(S)} \tag{5}$$

Based on a random binary image which has only two values; 0 for empty and 1 for filled, it can be described as

$$E(S^2) = \mathrm{var}(S) + E^2(S) \tag{6}$$

Plotnick et al. (1993) extended Eq. (5) into

$$\Lambda(r) = \frac{\mathrm{var}(S)}{E^2(S)} + 1 \tag{7}$$

where $E(S)$ is the mean and $\mathrm{var}(S)$ the variance of the number of occupied pixels per box.

4.2. Example (binary spatial patterns and lacunarity)

Fig. 3 shows six 15×15 binary image patterns, with white pixels representing 1's and black pixels representing 0's (gap). The lacunarity indices at different scales:

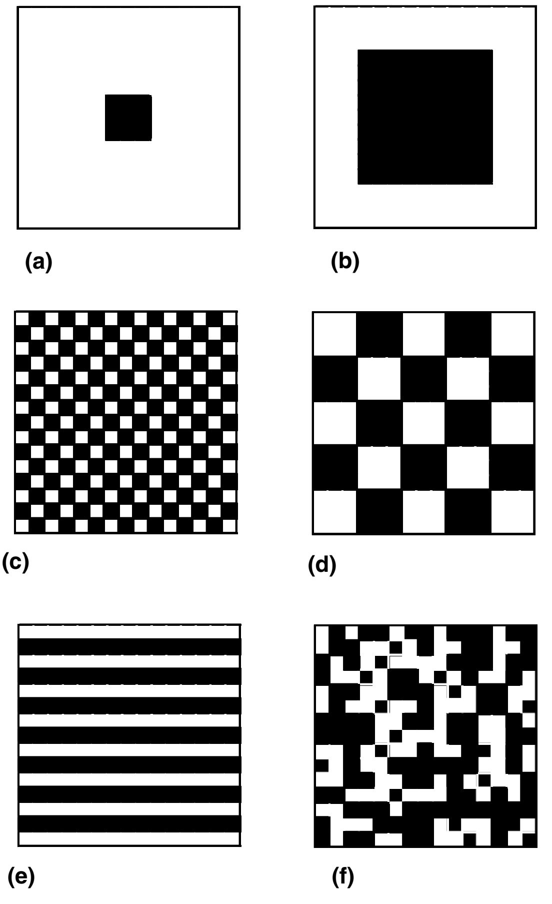

Fig. 3. Binary images of six spatial features: (a) small gap pattern, (b) big gap pattern, (c) small checker pattern, (d) big checker pattern, (e) small stripe pattern, (f) random pattern.

$r = 3, 5, 7, 9$, and 11 are computed for each pattern (Fig. 4). It can be observed that lacunarity measures the gappiness of scale dependent spatial features. For instance, pattern (b)—big gap (Fig. 3) has the biggest gap than other patterns, and lacunarity value is larger than that of others for almost all sizes since it contains many empty boxes. On the other hand pattern (c)–small checker is a regular pattern (i.e., translationally invariant), and the lacunarity value is close to 1, because the number of occupied pixels and empty pixels is constant at any location within a neighborhood. However, pattern (d)–big checker is also a regular pattern, which is similar to pattern (c) but at a coarser scale, does not give similar lacunarity value when using smaller gliding box sizes (e.g., 3×3). The lacunarity value of both patterns became closer to each other as the gliding box size increases. This situation is also true for pattern (a)—small gap and pattern (b)—big gap (again this can be consider a similar feature at a coarser scale), which shows significant differences in lacunarity values between

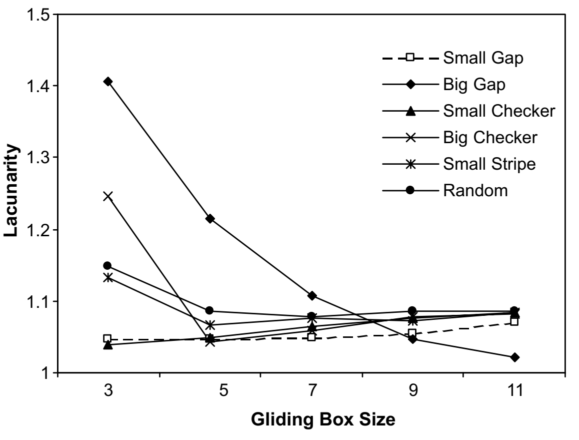

Fig. 4. Lacunarity curves of the six spatial features shown in Fig. 3 using the binary method.

the two patterns especially when using smaller gliding boxes. This apparently shows the scale dependency of lacunarity measures. Lacunarity binary approach characterizes pattern (c)—small checker, pattern (e)—small stripe, and pattern (f)—random with different lacunarity values when using smaller gliding boxes (see Fig. 4), but as gliding box sizes increase, their values become more similar. Hence, lacunarity can be used to measure different spatial patterns, but as any spatial/textural measures, lacunarity is highly scale dependent.

4.3. Lacunarity of gray-scale images

Lacunarity is not confined to binary configurations, but can also be used with gray scale data (Plotnick et al., 1996). Remotely sensed image data generally has three-dimensional structure (i.e., x-coordinate, y-coordinate, z-value). As discussed earlier, continuous image data can be transformed into four binary images by using the formula and threshold value to obtain lacunarity values. However, four binary images derived from one continuous image data are not true representative sets of the original image texture. Some valuable information on the spatial arrangements of objects or heterogeneity of complex texture features may be lost in the process of converting gray-scale images to binary images. Therefore, it was anticipated that lacunarity index value derived from original gray-scale images could provide better accuracy in texture based image classification.

Voss (1986) proposed a probability approach to estimate the fractal dimension and lacunarity of image intensity surface. The spatial arrangement of the points determines $P(m,L)$. $P(m,L)$ is the probability that there are m intensity points within a box size of L centered about an arbitrary point in an image. Intensity points are referred to as the number points filled in a cube box. Hence, we have

$$\sum_{m=1}^{N} P(m,L) = 1 \tag{8}$$

where N is the number of possible points in the box of L. Suppose that the total number of points in the image is M. If one overlays the image with boxes of side L, then the number of boxes with m points inside the box is $(M/m)P(m,L)$. Hence

$$M(L) = \sum_{m=1}^{N} mP(m,L) \tag{9}$$

and

$$M^2(L) = \underset{m=1}{\overset{N}{m}} m^2P(m,L) \tag{10}$$

Lacunarity can be computed from the same probability distribution $P(m,L)$. Hence, lacunarity $\Lambda(L)$ is defined as

$$\Lambda(L) = \frac{M^2(L) - (M(L))^2}{(M(L))^2} \tag{11}$$

A worked example for computing a lacunarity value is illustrated in Fig. 5. Texture transformed images of band 4, band 3, and band 2 derived from the gray-scale approach will be hereafter called V_4, V_3, and V_2. Example texture transformed image of IKONOS band 3 using the gray-scale approach with $3 \times 3 \times 3$ cube is shown in Fig. 6.

4.4. Effects of box sizes on lacunarity measures

To evaluate the effectiveness of box sizes, linear discriminant analysis approach was employed to identify four urban land use and land cover categories: agriculture, commercial, woodland, and R1. We generated 10 samples (33×33) for each of the above categories from the IKONOS image data and computed lacunarity index value for each sample using $3 \times 3 \times 3$, $5 \times 5 \times 5$, $7 \times 7 \times 7$, $9 \times 9 \times 9$, and $11 \times 11 \times 11$ cube sizes. Sample images of the four categories are shown in Fig. 7. The computed lacunarity values generated above were subject to discriminant analysis, and the results are shown in Table 1.

Discriminant analysis is useful for situations where we want to build a predictive model of group membership based on observed characteristics of each case. The procedure generates a discriminant function (or, for more than two groups, a set of discriminant functions) based on linear combinations of the predictor variables, which provide the best discrimination between the groups. The functions are generated from a sample of cases for which group membership is known; the functions can then be applied to new cases with measurements for the predictor variables but unknown group membership. The discriminant analysis was carried out to discriminate between classes of urban land cover samples on the basis of their lacunarity values (as predictor variables). Linear discriminant procedure was used to investigate the relative discriminatory power of all variables and to determine classification

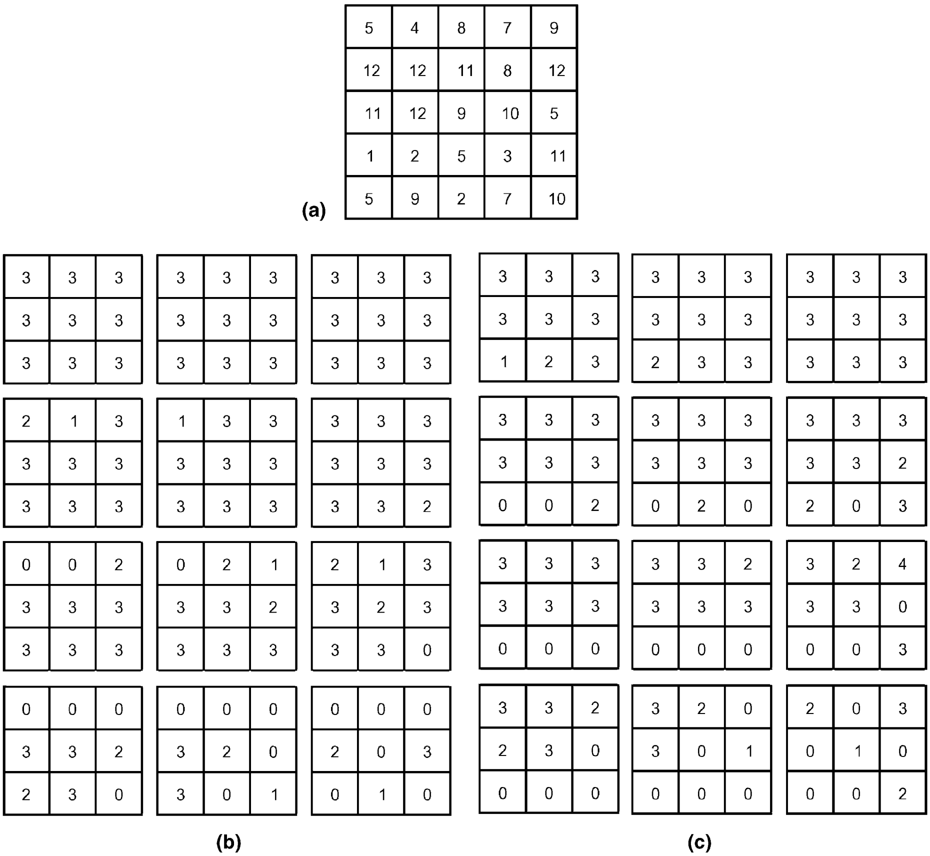

Fig. 5. A worked example to compute lacunarity value for a 5×5 image using $3 \times 3 \times 3$ cube size with gray-scale method: (a) a 5×5 original gray scale image, (b) intensity values for the first three rows, (c) intensity values for the second three rows, (d) intensity values for the third three rows, (e) sum of all intensity values in each cube box, (f) multiplication of total intensity value in each cube box and its probability value $[mP(m, L)]$, (g) multiplication of square of total intensity value in each cube box and its probability value $[m^2P(m, L)]$.

accuracies for different cube sizes (i.e., $3 \times 3 \times 3$, $5 \times 5 \times 5$, $7 \times 7 \times 7$, $9 \times 9 \times 9$, and $11 \times 11 \times 11$). In other words, the discriminant analysis was carried out to discriminate between textural features of the selected samples of the four classes on the basis of the lacunarity values using different cube sizes. This is an initial step towards understanding how robust the lacunarity approach with regards to varying cube sizes in discriminating samples (i.e., 33×33) of some selected classes. The most important information that we obtained from this step was the determination of the optimum cube size for real image classification.

Table 1 shows that box size of $3 \times 3 \times 3$ was the most accurate (overall accuracy of 67.5%), and this box size will be used to compute the lacunarity values in the

3	3	3	3	3	3	3	3	3
1	2	3	2	3	3	3	3	3
3	3	2	3	2	3	2	3	3
3	3	3	3	3	3	3	3	2
0	0	2	0	2	0	2	0	3
2	3	0	3	0	3	0	3	3
3	3	3	3	3	3	3	3	0
0	0	0	0	0	0	0	0	3
0	3	0	3	0	1	0	1	3
2	3	0	3	0	1	0	1	0
0	0	0	0	0	0	0	0	2
0	0	0	0	0	0	0	0	1

(d)

27	27	27	24	26	27	23	25	26
24	25	26	20	20	22	16	17	19
20	20	20	18	17	18	12	13	13
13	9	6	13	9	8	5	4	4

(e)

1.1	1.1	1.1	0.9	1.1	1.1	0.8	1.0	1.1
0.9	1.0	1.1	0.6	0.6	0.8	0.4	0.4	0.6
0.6	0.6	0.6	0.5	0.4	0.5	0.2	0.3	0.3
0.3	0.1	0.1	0.3	0.1	0.1	0.0	0.0	0.0

(f)

30.6	30.6	30.6	21.5	27.3	30.6	18.9	24.3	27.3
21.5	24.3	27.3	12.4	12.4	16.6	6.4	7.6	10.7
12.4	12.4	12.4	9.1	7.6	9.1	2.7	3.4	3.4
3.4	1.1	0.3	3.4	1.1	0.8	0.2	0.1	0.1

(g)

Fig 5 (*continued*)

Fig. 6. Example lacunarity index image of band 3 using the gray-scale method (29×29 local window with $3 \times 3 \times 3$ box).

following analysis. However, the difference in accuracy among the selected box sizes were not great, with the rest of the box sizes yielding slightly lower accuracies ranging from 57.5% to 50%. It can also be observed that the commercial samples gave the lowest user's and producer's accuracies for all cube sizes.

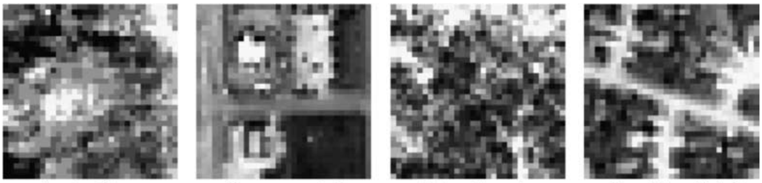

Fig. 7. Sample images of four land-use and land-cover classes displayed in band 3.

Table 1
Classification accuracy of lacunarity images derived from the gray-scale method using linear discriminant analysis

Category	Box size									
	$3 \times 3 \times 3$		$5 \times 5 \times 5$		$7 \times 7 \times 7$		$9 \times 9 \times 9$		$11 \times 11 \times 11$	
	Pro Acc	Usr Acc	Pro Acc	Usr Acc	Pro Acc	Usr Acc	Pro Acc	Usr Acc	Pro Acc	Usr Acc
A	100	83	90	82	90	82	90	82	80	73
C	30	43	20	25	10	14	10	17	20	25
F	80	60	60	55	70	58	70	54	60	46
R1	60	73	60	60	50	50	50	50	40	50
Ovr Acc		67.5		57.5		55.0		55.0		50.0

A = agriculture; C = commercial; F = woodland; R1 = residential-1; Pro Acc = producer's accuracy; Usr Acc = user's accuracy; Ovr Acc = overall accuracy.

5. Analysis

The computed values of both lacunarity approaches (i.e., lacunarity gray-scale, lacunarity binary) were assigned to the center pixel of the local moving window ($W \times W$), and the window moves throughout the whole image. The gray-scale method using different moving windows (i.e., 13×13, 21×21, 29×29) were employed to observe the nature and effectiveness of moving windows in characterizing urban texture features. It is expected that a 13×13 local window may be large enough to cover texture features of all selected land-use and land-cover types in this study. In other words, a distance of 13 pixels, in this case 52 m or 171 ft, may cover texture features of each land-use and land-cover class especially for the complex land-use classes such as residential and commercial. The most heterogeneous land use is residential category in this study. This is because this land use class generally contains a number of spectrally different pixels or objects. For example, features such as roads, houses, grasses, trees, bare soil, shrubs, driveways, swimming pools, and sidewalks, each of which may have a completely different spectral response, but together they are considered as a residential class. In other words, 52×52 m or 171×171 ft is large enough to cover a house, a sidewalk, a road, a driveway, a front yard, and a back yard to identify a residential class.

Window size apparently is not an issue for homogeneous classes. Criteria for the selection of window size were based on the resolution and the nature of the classes (homogeneity, size of the regions, characteristic scale, directionality, and spatial periodicity) to be identified. It should be noted that small window size (smaller than 13×13 for IKONOS image) may not cover sufficient spatial/texture information to characterize land-use and land-cover types. On the other hand, if the window size is too large, too much information from other land-use and land-cover features may be included and hence the discrimination result might not be accurate. Therefore, it is important to examine the appropriate window size for accurate discrimination of urban features (Myint, 2003b; Myint et al., 2002). We demonstrated from Fig. 4 and Table 1 that gliding box of 3×3 (for the binary approach) and $3 \times 3 \times 3$ cube (for the gray-scale approach) were more accurate than larger box sizes and cube sizes in discriminating land use land cover features. Hence, we decided to use 3×3 gliding box size for the binary approach and $3 \times 3 \times 3$ cube size for the gray-scale approach with the use of the selected window sizes (i.e., 13×13, 21×21, 29×29) to generate texture transformed images.

We used the combination of multi-spectral bands and their texture transformed images derived from all selected approaches. A supervised classification approach with the use of maximum likelihood classifier was employed to identify the classes in the study. The maximum likelihood decision rule is based on the probability that a pixel belongs to a particular class. The basic equation assumes that these probabilities are equal for all classes, and that the input data have normal distributions. Twenty-three training samples comprising about equal number of samples for each class (e.g., 3–4 training samples per class) were used in the classification for all band combinations. To better evaluate and for comparison purpose, the traditional multi-spectral band approach (i.e., C_4, C_3, C_2) was first employed. This is just to determine if traditional multi-spectral approach could provide satisfactory accuracy for urban classification, and whether we need texture analysis approaches to provide higher classification accuracy We then classified texture-transformed images of band 4, band 3, and band 2 derived from the lacunarity gray-scale approach, using a 29×29 local moving window. We did not include the original bands at this point since we wanted to observe the effectiveness of texture-transformed images alone in urban image classification. In our third analysis, we classified using different combinations of textural and original bands and the same window size. We analyzed the combination of C_4, C_3, C_2, V_4, V_3, and V_2 with the expectation that the combination of all original and transformed images could provide the highest accuracy. We also examined two other different alternatives: (1) C_4, C_3, C_2, and V_4, and (2) V_4, V_3, V_2, and C_4. The idea was to determine if one texture transformed band added to the original three bands and one original band added to the three texture transformed bands could provide satisfactory accuracy in image classification.

The best of all selected combinations, which gave the highest accuracy, was then used to determine the effectiveness of the selected local windows (i.e., 13×13, 21×21, 29×29). It is often suggested that it would be preferable to choose training sites, where possible, according to some stratified random sampling scheme. A minimum of 25 sample points per class using stratified random sampling technique was employed in the accuracy assessment. The identified random sample points were displayed on the original satellite image data with the help of local area knowledge, ground information collection, and existing land use maps of Norman to identify

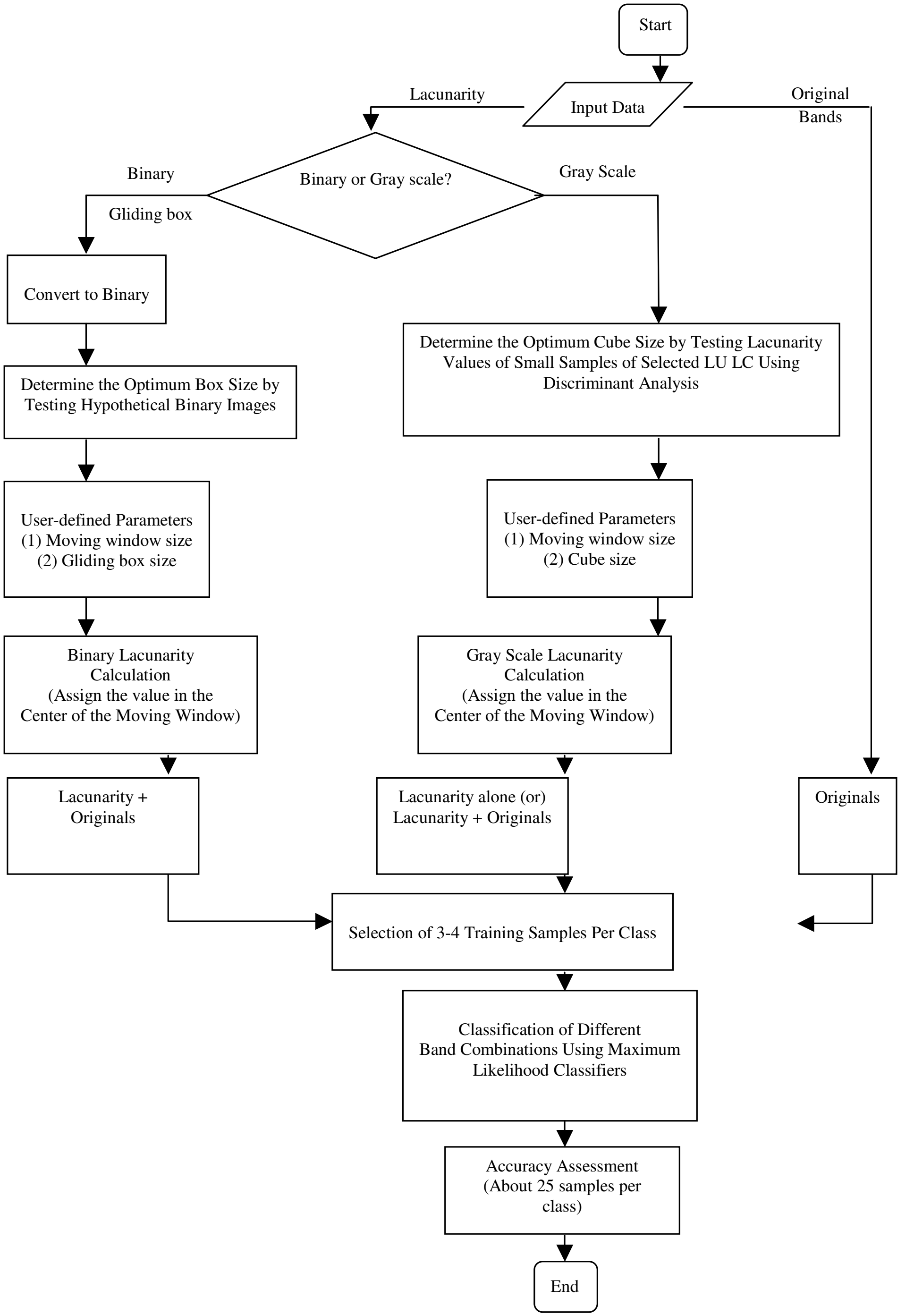

Fig. 8. Flow chart for the research procedure and design.

the classes. In order to be consistent with all approaches in urban image analysis and for comparison of classification accuracies, we used the same training samples, determined the same number of random samples for accuracy assessment, and employed the maximum likelihood algorithm for all band combinations. Both lacunarity approaches for texture analysis and image classification were developed using C++ programming language. Fig. 8 shows a flow chart demonstrating a complete procedure and research design of this study.

6. Results and discussion

It was found that traditional multi-spectral classification (i.e., band 4, band 3, band 2) was inaccurate for urban image classification from high-resolution data, since it produced 55% overall accuracy (Table 2). This is because spectral based classification approaches consider individual pixel value and ignore spatial arrangements of neighborhood pixels. As the spatial resolution of remotely sensed data gets finer, detailed objects and features in urban areas become more detectable (e.g., single family vs. multi family homes, roads, trees, parking lots, and so on); therefore, the spectral reflectance of an urban environment as a whole becomes more complex. Moreover, urban features are composed of spectrally diverse materials concentrated in a small area (e.g., plastic, metal, rubber, glass, cement, wood, and so on). In fact, the high frequency spatial appearance or complex nature of urban features may be the major limitation for using the spectral-based classification approaches in urban land-use and land-cover classification. For example, roads, houses, grasses, trees, bare soil, shrubs, swimming pools, driveway, and footpaths, each of which may have a completely different spectral response but may need to be considered together as a residential class. Hence, in order to identify urban land-use and land-cover classes we need to consider the spatial arrangements of neighborhood features and objects or texture and pattern, in addition to considering individual pixel values (Myint et al., 2002, in press).

After adding texture-transformed image of band 4 (V_4) to the original multi-spectral bands (i.e., C_4, C_3, C_2), the overall classification accuracy was increased from 55% to 84%. As mentioned earlier we also tested texture transformed images alone generated from the lacunarity gray-scale method using a 29×29 local window. It was found that the combination of texture transformed images alone was not so effective since it gave only 68% overall accuracy. It can also be observed from Table 2 that one texture transformed image added to the original spectral bands ($C_4 + C_3 + C_2 + V_4$) was more accurate than one original band added to the texture transformed bands ($V_4 + V_3 + V_2 + C_4$). In other words, one additional texture information added to the three original bands could provide better accuracy than one original band added to the three texture transformed images. Combining all of the original spectral bands and their texture-transformed images was the best approach since it achieved 92.0% accuracy.

We also used the best band combination approach to examine two other window sizes (i.e., 13×13, 21×21). It was found that the 13×13 and 21×21 window sizes

Table 2
Classification accuracy of different original and texture transformed band combinations

Category	Band combination									
	$C_4 + C_3 + C_2$		$V_4 + V_3 + V_2$		$C_4 + C_3 + C_2 + V_4$		$V_4 + V_3 + V_2 + C_4$		$C_4 + C_3 + C_2$, $V_4 + V_3 + V_2$	
	Pro Acc	Usr Acc	Pro Acc	Usr Acc	Pro Acc	Usr Acc	Pro Acc	Usr Acc	Pro Acc	Usr Acc
A	48	53	48	100	46	100	47	94	77	100
R1	43	57	72	77	91	78	86	67	89	89
R2	37	83	74	77	82	88	84	82	94	94
W	100	85	0	0	100	100	100	100	100	100
G	100	20	93	47	100	48	100	17	95	75
F	100	43	100	63	100	88	88	88	94	100
C	70	53	63	87	95	98	64	87	98	95
Ovr Acc		55.0		67.5		84.0		74.5		92.0

A = agriculture; R1 = residential-1; R2 = residential-2; W = water; G = grassland; F = woodland; C = commercial; Pro Acc = producer's accuracy; Usr Acc = user's accuracy; Ovr Acc = overall accuracy.

gave lower accuracies than the 29×29 window, 88.0% and 86.5%, respectively (Table 3). Even though the 29×29 window was found to be the best among all three window sizes, it does not necessarily mean that this window size is the most effective local window size in urban image classification, and further testing is needed to examine how this window size will behave using other types of images. A much larger window may cover more texture information from other land-use and land-cover features and could consequently lead to poor classification accuracy.

From Table 4, the second highest classification accuracy was produced by the lacunarity-binary approach with an overall accuracy of 81%, which is below the minimum mapping accuracy of 85% required for most resource management applications (Townshend, 1981). In fact, the lacunarity gray-scale approach with a

Table 3
Classification accuracy of 13×13, 21×21, and 29×29 window sizes using the best band combination ($C_4 + C_3 + C_2 + V_4 + V_3 + V_2$)

Category	Local moving window size					
	13×13		21×21		29×29	
	Pro Acc	Usr Acc	Pro Acc	Usr Acc	Pro Acc	Usr Acc
A	68	100	53	100	77	100
R1	85	74	95	93	89	89
R2	82	86	98	89	94	94
W	100	100	100	100	100	100
G	90	68	73	46	95	75
F	95	100	100	100	94	100
C	94	96	95	93	98	95
Ovr Acc		86.5		88.0		92.0

A = agriculture; R1 = residential-1; R2 = residential-2; W = water; G = grassland; F = woodland; C = commercial; Pro Acc = producer's accuracy; Usr Acc = user's accuracy; Ovr Acc = overall accuracy.

Table 4
Classification accuracy of original bands, combination of original bands and texture transformed images generated by the binary method, and combination of original bands and texture transformed images generated by the gray-scale method

Category	Original and spatial transformed images (29×29 windows)					
	Original bands		Lacunarity (binary)		Lacunarity (Voss)	
	Pro Acc	Usr Acc	Pro Acc	Usr Acc	Pro Acc	Usr Acc
A	48	53	63	100	77	100
R1	43	57	73	73	89	89
R2	37	83	78	97	94	94
W	100	85	100	100	100	100
G	100	20	100	43	95	75
F	100	43	100	83	94	100
C	70	53	85	77	98	95
Ovr Acc		55.0		81.0		92.0

A = agriculture; R1 = residential-1; R2 = residential-2; W = water; G = grassland; F = woodland; C = commercial; Pro Acc = producer's accuracy; Usr Acc = user's accuracy; Ovr Acc = overall accuracy.

13×13 window produced even higher accuracy (86.5%) than the binary approach with a 29×29 window. This may be due to the fact that much texture information might have been lost when converting from the original image to four binary images (i.e., Q_1, Q_2, Q_3, Q_4).

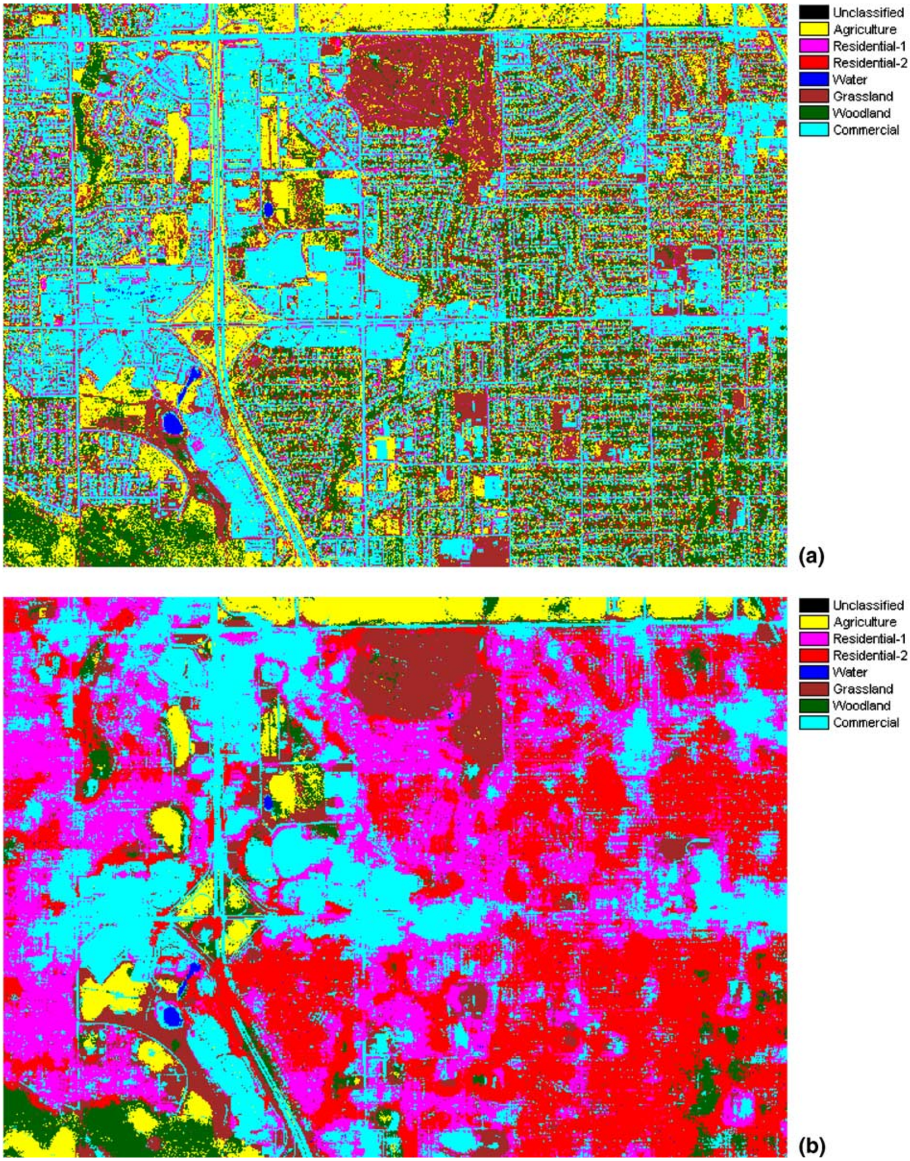

Fig. 9. Output maps: (a) traditional spectral approach; (b) lacunarity gray-scale. (Note: the same training samples, the same classification approach, and the same class colors used.)—For interpretation of color in this figure legend the reader is referred to the web version of this article.

In examining the accuracy of land-cover types, it can be observed that there is some confusion between agriculture and grassland. This is because they both are spectrally and spatially related to similar feature classes. In general, they were the two categories which made our classification accuracy lower. The only highly reliable category found was water in this study. It reaches the highest user's and producer's accuracy (100%) for all approaches, all window sizes, and all band combinations. The output maps from the traditional multi-spectral approach and the lacunarity gray-scale approach are shown in Fig. 9(a) and (b), respectively. As mentioned earlier, we used the same training samples, same number of random points for accuracy assessment, and same classification algorithm for all approaches. We also applied same color scheme to each category in the output maps: yellow for agriculture, cyan for commercial, green for woodland, black for water, purple for R1, red for R2.

7. Conclusions

This study shows that traditional spectral based classification approach alone does not provide sufficient accuracy in classifying urban land categories from high-resolution image data. Lacunarity as a texture measure can be used to improve the classification accuracy dramatically. It should be noted, however, that the selection of local moving window size and gliding box size (issue of scale) plays an important role in determining accuracy in characterizing spatial features for urban image classification. Hence, future study should focus on more in-depth evaluation of window sizes and gliding box sizes and their effects on different types of land use land cover classification. Other lacunarity approaches (Dong, 2000; Keller, Chen, & Crownover, 1989) could also be explored and examined in future study. This approach can be adopted to improve any land use and land cover classification study dealing with heterogeneous features or to discriminate categories, which are statistically similar but possessing different patterns and textures.

Acknowledgment

The research presented in this paper was supported in part by a NASA EPSCoR grant received through the Oklahoma Space Grant Consortium.

References

Allain, C., & Cloitre, M. (1991). Characterizing the lacunarity of random and deterministic fractal sets. *Physics Review A, 44*, 552–3558.

Barnsley, M. J., Barr, S. L., & Sadler, G. J. (1991). Spatial re-classification of remotely sensed images for urban land-use monitoring. In *Proceedings of Spatial Data 2000* (pp. 106–117). Nottingham, Oxford: Remote Sensing Society, 17–20 September.

Burrough, P. A. (1989). In D. Avnir (Ed.), *Fractal and geochemistry, the fractal approach to heterogeneous chemistry* (pp. 383–405). New York: Wiley.

Burrough, P. A. (1993). Soil variability: A late 20th century view. *Soils and Fertilizers*, 529–562.

De Cola, L. (1989). Fractal analysis of a classified Landsat scene. *Photogrammetric Engineering and Remote Sensing, 55*, 601–610.

De Jong, S. M., & Burrough, P. A. (1995). A fractal approach to the classification of Mediterranean vegetation types in remotely sensed images. *Photogrammetric Engineering and Remote Sensing, 61*, 1041–1053.

Dong, P. (2000). Lacunarity for spatial heterogeneity measurement in GIS. *Geographic Information Sciences, 6*(1), 20–26.

Emerson, C. W., Lam, N. S. N., & Quattrochi, D. A. (1999). Multi-scale fractal analysis of image texture and pattern. *Photogrammetric Engineering and Remote Sensing, 65*(1), 51–61.

Franklin, S. E., Hall, R. J., Moskal, L. M., Maudie, A. J., & Lavigne, M. B. (2000). Incorporating texture into classification of forest species composition from airborne multispectral images. *International Journal of Remote Sensing, 21*(1), 61–79.

Gallo, K. P., McNab, A. L., Karl, T. R., Brown, J. F., Hood, J. J., & Tarpley, J. D. (1993). The use of a vegetation index for assessment of the urban heat island effect. *International Journal of Remote Sensing, 14*(11), 2223–2230.

Gefen, Y., Meir, Y., & Aharony, A. (1983). Geometric implementation of hypercubic lattices with noninteger dimensionality by use of low lacunarity fractal lattices. *Physical Review Letters, 50*, 145–148.

Green, D. R., Cummins, R., Wright, R., & Miles, J. (1993). A methodology for acquiring information on vegetation succession from remotely sensed imagery. In R. Haines-Young, D. R. Green, & S. Cousins (Eds.), *Landscape Ecology and Geographic Information Systems* (pp. 111–128). London: Taylor and Francis.

Gustafson, E. J. (1998). Quantifying landscape spatial pattern: What is the state of the art? *Ecosystems, 1*, 143–156.

Haines-Young, R., & Chopping, M. (1996). Quantifying landscape structure: A review of landscape indices and their application to forested landscapes. *Progress in Physical Geography, 20*, 418–445.

Haralick, R. M, Shanmugan, K., & Dinstein, J. (1973). Textural features for image classification. *IEEE Transaction on Systems, Man, and Cybernetics, SMC-3*(6), 610–621.

Huang, Y. J., Akbari, H., Taha, H., & Rosenfeld, A. H. (1987). The potential of vegetation in reducing summer cooling loads in residential buildings. *Journal of Climate and Applied Meteorology, 26*, 1103–1116.

Jaggi, S., Quattrochi, D. A., & Lam, N. S. N. (1993). Implementation and operation of three fractal measurement algorithms for analysis of remote-sensing data. *Computer and Geosciences, 19*(6), 745–767.

Jensen, J. R., & Cowen, D. C. (1999). Remote sensing of urban/suburban infrastructure and socio-economic attributes. *Photogrammetric Engineering and Remote Sensing, 65*(5), 611–622.

Kaplan, L. M. (1999). Extended fractal analysis for texture classification and segmentation. *IEEE Transactions on Image Processing, 8*, 1527–1585.

Keller, J. M., Chen, S., & Crownover, R. M. (1989). Texture description and segmentation through fractal geometry. *Computer Vision, Graphics, and Image Processing, 45*, 150–166.

Kiema, J. B. K., & Bahr, H. P. (2001). Wavelet compression and the automatic classification of urban environments using high resolution multispectral imagery and laser scanning data. *GeoInformatica, 5*(2), 165–179.

Klinkenberg, B., & Goodchild, M. F. (1992). The fractal properties of topography: A comparison of methods. *Earth Surface Processes and Landforms, 17*, 217–234.

Lam, N. S. N. (1990). Description and measurement of Landsat TM images using fractals. *Photogrammetric Engineering and Remote Sensing, 56*(2), 187–195.

Lam, N. S. N., Quattrochi, D., Qui, H., & Zhao, W. (1998). Environmental assessment and monitoring with image characterization and modeling system using multiscale remote sensing data. *Applied Geographic Studies, 2*(2), 77–93.

Lin, B., & Yang, Z. R. (1986). A suggested lacunarity expression for Sierpinski carpets. *Journal Physics A: Mathematical and General, 19*, L49–L52.

Lo, C. P., Quatrochi, D. A., & Luvall, J. C. (1997). Application of high-resolution thermal infrared remote sensing and GIS to assess the urban heat island effect. *International Journal of Remote Sensing, 18*(2), 287–304.

Lovejoy, S., & Schertzer, D. (1990). Multifractals, universality classes and satellite and radar measurements of cloud and rain fields. *Journal of Geophysical Research, 95*, 2021–2034.

Mandelbrot, B. B. (1983). *The fractal geometry of nature*. New York: Freeman and Co.

Mandelbrot, B. (1995). Measures of fractal lacunarity: Minkowski content and alternatives. *Progress in Probability, 37*, 15–42.

Mark, D. M., & Aronson, P. B. (1984). Scale dependent fractal dimensions of topographic surfaces: An empirical investigation with applications in geomorphology and computer mapping. *Mathematical Geology, 16*, 671–683.

Metzger, J. P., & Muller, E. (1996). Characterizing the complexity of landscape boundaries by remote sensing. *Landscape Ecology, 11*, 65–77.

Muller, E. (1997). Mapping riparian vegetation along rivers: old concepts and new methods. *Aquatic Botany, 58*, 411–437.

Myint, S. W. (2003a). Fractal approaches in texture analysis and classification of remotely sensed data: Comparisons with spatial autocorrelation techniques and simple descriptive statistics. *International Journal of Remote Sensing, 24*(9), 1925–1947.

Myint, S. W. (2003b). The use of wavelets for feature extraction of cities in satellite images. In V. Mesev (Ed.), *Remotely sensed cities* (pp. 109–134). London: Taylors and Frances.

Myint, S. W., Lam, N. S. N., & Tyler, J. (2002). An evaluation of four different wavelet decomposition procedures for spatial feature discrimination within and around urban areas. *Transactions in GIS, 6*(4), 403–429.

Myint, S. W., Lam, N. S. N., & Tyler, J. (in press). Wavelet for urban spatial feature discrimination: Comparisons with fractal, spatial autocorrelation, and spatial co-occurrence approaches. *Photogrammetric Engineering and Remote Sensing*.

Oke, T. R. (1982). The energetic basis of the urban heat island. *Quarterly Journal of the Royal Meteorological Society, 108*, 1–24.

Owen, T. W., Carlson, T. N., & Gillies, R. R. (1998). An assessment of satellite remotely sensed land cover parameters in quantitatively describing the climatic effect of urbanization. *International Journal of Remote Sensing, 19*(9), 1663–1681.

Peddle, D. R., & Franklin, S. E. (1991). Image texture processing and data integration for surface pattern discrimination. *Photogrammetric Engineering and Remote Sensing, 57*, 413–420.

Pesaresi, M. (2000). Texture analysis for urban pattern recognition using fine-resolution panchromatic satellite imagery. *Geographical and Environmental Modelling, 4*(1), 43–63.

Plotnick, R. E., Gardner, R. H., Hargrove, W. W., Prestegaard, K., & Perlmutter, M. (1996). Lacunarity analysis: A general technique for the analysis of spatial patterns. *Physical Review E, 53*, 5461–5468.

Plotnick, R. E., Gardner, R. H., & O'Neill, R. V. (1993). Lacunarity indices as measures of landscape texture. *Landscape Ecology, 8*, 201–211.

Roach, D., & Fung, K. B. (1994). Fractal-based textural descriptors for remotely sensed forestry data. *Canadian Journal of Remote Sensing, 20*, 59–70.

Sadler, G. J., Barnsley, M. J., & Barr, S. L. (1991). Information extraction from remotely-sensed images for urban land analysis. In: *Proceedings of the Second European Conference on Geographical Information Systems (EGIS'91)* (pp. 955–964) April, Brussels, Belgium, Utrecht: EGIS Foundation.

Townshend, J. R. G. (1981). *Terrain analysis and remote sensing*. London: George Allen and Unwin, 272 p.

Turcotte, D. (1997). *Fractals and chaos in geology and geophysics* (2nd ed.). Cambridge: Cambridge University Press, 412 p.

Voss, R. (1986). Random fractals: characterization and measurement. In R. Pynn & A. Skjeltorp (Eds.), *Scaling phenomena in disordered systems*. New York: Plenum.

Wagrowski, D. M., & Hites, R. A. (1997). Polycyclic aromatic hydrocarbon accumulation in urban, suburban and rural vegetation. *Environmental Science & Technology, 31*(1), 279–282.

Xia, Z. (1993). *The Uses and Limitations of Fractal Geometry in Digital Terrain Modelling* (252 p.). Ph.D. Thesis, City University of New York.